
# Bond graph model of a switched reluctance machine

| | |
|---|---|
| Journal: | *Transactions on Industrial Electronics* |
| Manuscript ID: | 09-1152-TIE |
| Manuscript Type: | Regular paper |
| Manuscript Subject: | Machines and Drives |
| Keywords: | Electric machines, Reluctance machines, Modeling |
| Are any of authors IEEE Member?: | No |
| Are any of authors IES Member?: | No |
| | |


For Review

# Bond graph model of a switched reluctance machine

***Abstract*—This paper presents an energy-based model of a switched reluctance machine (SRM), using the bond graph formalism. The IC-element, which can be applied to describe the electromechanical energy transformation in electrical machines, is used for a SRM. The bond graph model for a generalized SRM is introduced. The generalized case is particularized and implemented, using the 20sim software, for a 6/4 SRM machine, and simulations are then performed. Experimental characteristics curves can be also included in the bond graph model, and they are used to compare the behaviour of a real SRM plant with that obtained via simulations. The obtained model is a modulable bond graph, which can be modified depending on the simulation requirements. Another advantage, due to the use of the bond graph modelling, is the ability of the same model to operate as a motor or generator.**

***Index Terms*—Switched reluctance machines, modeling, bond graph.**

## I. Introduction

Switched reluctance machines (SRM) have emerged as a popular alternative to brushless DC and AC motors because of its simple and reliable structure, *i.e.*, no magnets and windings on the rotor [1]. One of the main advantages of the SRM is that they can produce high motor torque at low speeds. SRM are present in many home applications (washing machines, door actuators), robotics, automotive applications and recently in hybrid electrical vehicles [2] or flywheel energy storage systems [3]. However, they are not yet widely accepted due to the non-linear nature of its torque production, which causes torque ripples [4] and thereby vibrations and noise.

Modeling has become one of the main topics in SRM research [5]. Neural networks have been proposed to describe a SRM under a fail mode operation [6]. In [7] a model containing the mutual coupling between phases has been presented. Another example is [8], where an autocalibration strategy is adopted to update the inductance values. In this work a bond graph approach to SRM modeling will be presented. The main advantage is that the obtained model can be easily modified depending on the required complexity, from the linear and classic non-saturated model to the more complex description including the nonlinear nature of the electromagnetic coupling field, or as it will be shown in this paper, using the experimental magnetization curves obtained from a real plant. Besides, the bond graph description permits the integration of submodels easily (such as a power converter model or mechanical loads) and, by means of a simple computer algorithm, the simulation-ready equations of a complex model can be obtained.

The bond graph formalism is a graphical approach to modeling, based on the concept of power and incorporating ideas from network theory in a general setting [9][10]. The systems are modeled as a set of elements which exchange energy in a power-conserving way. Generally, the models obtained in this framework, besides being noncausal, are inherently modular and correspond to the physical system more closely than in the more prevalent, signal-based modeling paradigm.

Given a bond graph model, causality can be assigned and algebraic-differential equations can then be obtained in an algorithmic way.

Bond graph modeling is a multi-domain approach that has been applied in a variety of disciplines, covering all areas of engineering but also many others such as biological systems [11]. To name just a few applications, bond graphs have been used to model electrical, mechanical, magnetic, hydraulic and thermofluidic systems (see examples in [10]), or more complex systems as a water rocket systems [12], and also variable structure systems as power converters [13]. Bond graph models, being intrinsically modular, have also been used to describe large and complex systems, such as four-wheel vehicles with electrically controlled brakes and steering [14], hybrid electric vehicles [15] or hybrid railway traction systems [16].

Electrical machines are a natural area of application for bonds graphs, as they connect the electrical and mechanical domains. Examples include DC machines [10], simple AC machine [17], three-phase machines, both induction ones [18] and synchronous [19], or some other more exotic systems as the Jeffcott rotor [20]. The electromagnetic coupling between the electrical and the mechanical domains has been also studied in detail in this formalism. In [21] saturation effects and nonlinearities were included in a bond graph model of a claw-pole alternator. A comparative study between a bond graph model and a finite element approach has been done in [22].

This paper is organized as follows. In Section II, the bond graph theory and the electromechanical energy conversion core element is introduced. The generalized description of the switched reluctance machine (SRM) is done in Section III. Then, the bond graph model of a 6/4 SRM is obtained in Section IV and its implementation and simulations into an specific software are also presented. In Section V an experimentally-based model, using the magnetization curves of a real 6/4 SRM, is compared with the behaviour of a real machine. Finally, Section VI, states the conclusions of this work.

## II. The bond graph theory

Bond graph theory describes the power exchange between the elements of a system. The energy exchange is represented by means of a power bond, depicted as a half arrow, connecting the power ports of two elements (see Fig. 1). Associated to each bond there is a pair of signals ($e$, effort, and $f$, flow) such that their product yields the power flowing from one element to the other. Each physical domain has an effort and a flow

For Peer Review

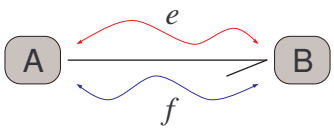


Fig. 1. The power bond describes the energy exchange between two elements.

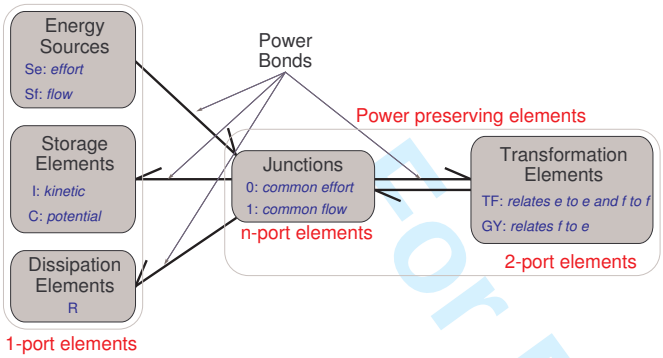


Fig. 2. Primary elements of the bond graph formulation.

variable, *e.g.* voltage and current in the electrical domain, or force and velocity in the mechanical domain.

In a generalized form, power bonds are $n$-dimensional power links between the connected elements. A classic electric example can be found in three-phase electrical systems, which can be represented using only one power bond which contains three voltages and currents.

An important fact of the bond graph modeling, due to the energy-based description, is the ability to obtain reusable models. An example of this property is presented in this paper, where the built SRM bond graph model can be used both as a motor and as a generator.

### A. Elements

Basic bond graph theory is summarized in Fig. 2. This modelling language is based on the interconnection, by means of power bonds, of different kinds of elements, which can be classified as energy sources, storage elements and dissipative elements. Transformation elements represent a power preserving modification of the energy flowing between two elements. All these elements are connected trough a network build using junction elements. Electrical domain examples of each element can help to describe the physical nature of the primary bond graph elements:

- 1-port elements
  - Energy sources, Se and Sf: voltage and current sources, respectively.
  - Storage elements, C and I: capacitors and inductors, respectively.
  - Dissipative elements, R: resistors.
- 2-port elements
  - Transformer, TF: ideal transformer.
  - Gyrator, GY: ideal DC-machine.
- n-port elements
  - 0-junction: all the connected elements have the same effort, Kirchhoff voltage law.
  - 1-junction: all the connected elements have the same flow, Kirchhoff current law.

All the elements can be modualted by signals, also called activated bonds, which do not carry any power. This can be used to represent external events (usually not described by an energy effect), such as an externally regulated voltage source or variable resistors.

### B. Causality

Causality is a fundamental aspect in the bond graph formulation, and it is required in order to obtain the dynamical equations. It defines the signal process associated to the model, or in other words, it dictates what are the input and output variables of an element. Causality is indicated in the bond graph by the causal stroke, and it determines which element fixes the effort. Causality does not depend on the power direction, and it depends on the interconnected elements.

Causality can be easily fixed by a set of rules. There are fixed causality elements (sources), constrained causality elements (TF, GY and junctions), preferred causality elements (C and I elements) or indifferent causality elements (R elements). Combination of these causal laws yields the causal assignation required by the simulator to generate the algebraic-differential dynamical equations.

Causality assignment is a post-process, and it is carried out after the complete model is assembled. This conferes the formalism the ability to obtain reusable models which are valid for different causal assignations. Once the model is connected with other elements, causality is automatically fixed and the dynamics can be computed. An example of this property is presented in this paper, where the obtained SRM bond graph model can be used both as a motor and as a generator.

### C. The IC-element

Electrical domain systems with constitutive relations depending on geometric parameters develop additional mechanical ports through which power can flow and be exchanged with the electrical ports. Here we will cast the expressions for the constitutive laws of the ports into the bond graph form. Unfortunately, the elemental primary elements introduced above cannot describe this behaviour, and the use of the IC-field is adopted to represent the called *coupling field* [23] in an electromechanical system.

From the primary elements, more complex elements can be defined. One of them is the IC-element (Fig. 3), which consist in a field of I and C elements, internally connected [10]. The IC element is the standard way of representing in bond graph theory a system where some of the state variables are driven by efforts (the I part), and some by flows (the C part), which is the case of the magnetic coupling in a electrical machine [17].

For Peer Review

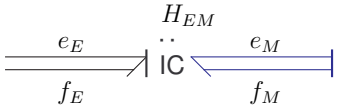


Fig. 3. Bond graph of a generalized electromechanical system.

The IC-element, in a general description[1], contains $n_E$ electrical ports $(e_E, f_E)$ and $n_M$ mechanical ones $(e_M, f_M)$, and the state variables are denoted by $p_E \in \mathbb{R}^{n_E}$ and $q_M \in \mathbb{R}^{n_M}$.

The dynamics of the state variables are driven by the corresponding power variables:

$$\dot{p}_E = e_E \quad (1)$$
$$\dot{q}_M = f_M, \quad (2)$$

while the dual power variables at each port can be obtained from the energy function, or Hamiltonian, $H_{EM} = H_{EM}(p_E, q_M)$, yielding the constitutive relationships of the system[2]:

$$f_E = \partial_{p_E} H_{EM} \quad (3)$$
$$e_M = \partial_{q_M} H_{EM} \quad (4)$$

Notice that the existence of an energy function $H_{EM}$ depends on the fulfilling of Maxwell's reciprocity relations. Indeed, from (3) and (4), and assuming sufficiently smooth functions,

$$\partial_{q_M} f_E = \partial_{p_E} e_M.$$

Thus, given $f_E(p_E, q_M)$ one can compute $e_M(p_E, q_M)$, or the other way around; this is frequently exploited when computing forces or torques in electromechanical systems, as will be explained below in more detail.

## III. The Switched Reluctance Machine

Fig. 4 shows a cross section scheme of one of the most typical configurations, the 6/4 switched reluctance machine. The different number of poles, 6 for the stator and 4 for the rotor, allows to start and operate in both directions.

The SRM requires an specific drive circuit which supplies each phase coil with a switched voltage. This power electronic supply plays an important role in the torque production, since each phase must be switched on and turned off depending on the rotor position. Fig. 5 displays the SRM and its associated classic power converter. Notice that the knowledge of the rotor position is required to generate the appropriate voltages.

Although the power converter is an important part of any working SRM, in this work we only focus on the bond graph description of the electromechanical part. For simulation purposes we consider controlled ideal voltage sources with the appropriate voltage signals. This is assumed since the power converter dynamics is much faster than the electrical one.

[1]Here we denote $E$ and $M$ subindexes, for electrical and mechanical ports respectively, for a later use in the SRM model

[2]In this paper, to simplify the notation, the $\frac{\partial f}{\partial x}(x)$ operations has been also defined as $\partial_x f(x)$ and is considered as a column vector.

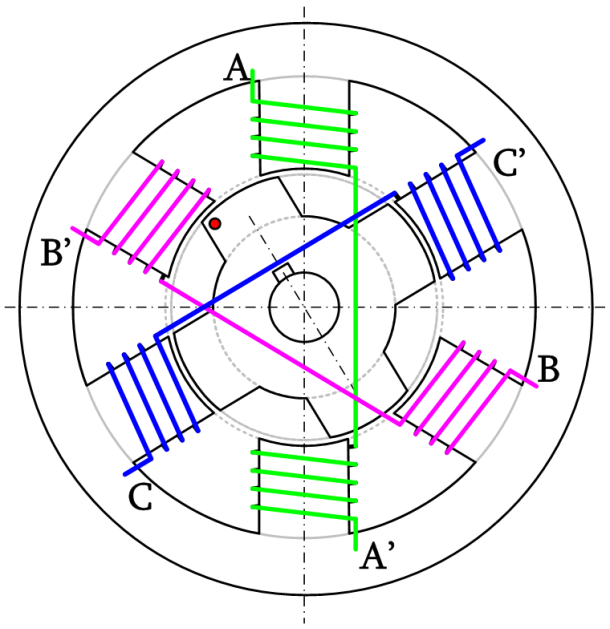


Fig. 4. Scheme of a cross section for a 6/4 switched reluctance machine.

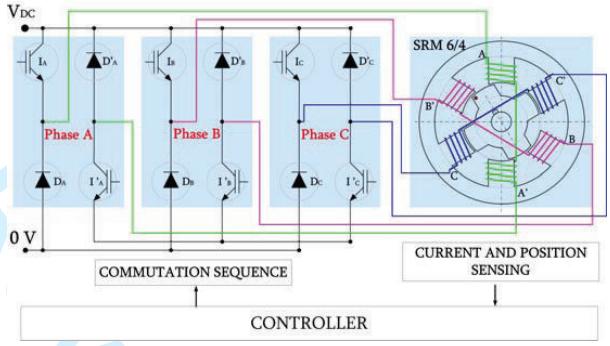


Fig. 5. Driver scheme for a 6/4 switched reluctance machine.

### A. SRM dynamics

The electrical equations are given by

$$V = Ri + \dot{\lambda} \quad (5)$$

where $V \in \mathbb{R}^n$ are the voltages applied to the stator windings, $i \in \mathbb{R}^n$ are the currents, $\lambda \in \mathbb{R}^n$ are the fluxes, $R = \text{diag}\{r_1, r_2, \ldots, r_n\} \in \mathbb{R}^{n \times n}$ is the resistance matrix (where $r$ is the resistance of each stator winding) and $n$ denotes the number of stator phases.

The relationship between the energy and co-energy variables is described by the inductance matrix

$$\lambda = \mathcal{L}(\theta, i)i. \quad (6)$$

This is a complex function which involves saturation and nonlinear effects, as well as cross terms between different phases. As explained below, the $\mathcal{L}(\theta, i)$ matrix description is essential to obtain an appropriate model, because it directly appears in the electrical torque and current equations. In this paper two descriptions of the inductance matrix will be used; the widely accepted linear case, in Section IV, and an experimentally-based model, Section V.

For Peer Review

The magnetic energy is given by

$$H_{EM} = \frac{1}{2}\lambda^T \mathcal{L}^{-1}\lambda, \tag{7}$$

and the mechanical equation is

$$\tau_L = J\dot{\omega} + b\omega + \tau_e \tag{8}$$

where $\omega$ is the mechanical speed, $\tau_L$ is an external torque, $\tau_e$ is the electrical torque, $J$ is the rotor inertia, and $b$ represents the viscous damping. The electrical torque $\tau_e$ is produced by the interaction of the magnetic fields, *i.e.* it can be written from the magnetic energy (7), as

$$\tau_e = \partial_\theta H_{EM} \tag{9}$$

or, tacking into account the quadratic form of (7)

$$\tau_e = \frac{1}{2}\lambda^T \partial_\theta(\mathcal{L}^{-1})\lambda. \tag{10}$$

## IV. The SRM bond graph model

The SRM electrical dynamics consists in a set of RL circuits with a $\theta$-depending inductances and saturation effects. It implies that the SRM is a higher nonlinear system. Disregarding nonlinear effects in the mechanical damping or in the electrical resistances (like dry friction or temperature effects), nonlinearities are only present in the inductance matrix. As it is shown in the previous Section, the choice of the inductance matrix will determine also the produced torque model. This fact implies that the model accuracy will basically depend on the adopted model of the $\mathcal{L}$ matrix.

The easiest, and widely accepted, model for a SRM machine is defined by a non-saturated and magnetically decoupled inductance matrix, which also disregards higher first harmonics. In this Section a bond graph model for a SRM is developed, and the particular 6/4 configuration is implemented and validated via simulations.

### A. Inductance matrix definition

As pointed out in Section III, the inductance matrix relates currents and fluxes. A commonly accepted relationship between these variables is the following function

$$\lambda = \mathcal{L}(\theta)i, \tag{11}$$

where the variables are linearly dependent for a given rotor position $\theta$. The SRM is commonly designed to be magnetically decoupled [1]. Using this fact, the mutual inductances are neglected, and the inductance matrix can be written as

$$\mathcal{L}(\theta) = \begin{bmatrix} L_1(\theta) & 0 & \dots & 0 \\ 0 & L_2(\theta) & \dots & 0 \\ \vdots & \vdots & \ddots & \vdots \\ 0 & 0 & \dots & L_n(\theta) \end{bmatrix}. \tag{12}$$

In a first approximation, it is usual practice to describe each phase inductance function as a Fourier series expansion and keep then only the first harmonic component. Then,

$$L_j = l_0 - l_1 \cos\left(N_r\theta + (j-1)\frac{2\pi}{n}\right) \tag{13}$$

where $j = 1, \dots, n$, $\theta$ is the rotor position, $N_r$ is the number of rotor poles, and $l_0$ and $l_1$ are constants corresponding to the zero and the first harmonic components. In this case, the $l_0$ and $l_1$ inductance constants corresponds to the inductance value at the alignment position and the non-alignment positions, respectively.

Many inductance functions have been proposed for modeling SRM [1]. In this Section we use the first Fourier approximation, which is the most commonly accepted form. In the next Section, the inductance functions are replaced by experimental curves, and they are used in the bond graph. Notice that, as explained below, any nonlinear function can be adopted as the inductance function (it must be differentiable for all $\theta$ values).

As explained in the previous section, the magnetic energy is a quadratic form (7), and consequently the produced torque is given by (10). From (12), and due to the mutual inductances are neglected, the $\partial_\theta(\mathcal{L}^{-1})$ matrix can be easily computed as

$$\partial_\theta(\mathcal{L}^{-1}) = \begin{bmatrix} \partial_\theta(L_1^{-1}) & 0 & \dots & 0 \\ 0 & \partial_\theta(L_2^{-1}) & \dots & 0 \\ \vdots & \vdots & \ddots & \vdots \\ 0 & 0 & \dots & \partial_\theta(L_n^{-1}) \end{bmatrix}, \tag{14}$$

where

$$\partial_\theta(L_j^{-1}) = -\frac{l_1 N_r \sin\left(N_r\theta + (j-1)\frac{2\pi}{n}\right)}{\left(l_0 - l_1\cos\left(N_r\theta + (j-1)\frac{2\pi}{n}\right)\right)^2} \tag{15}$$

for $j = 1, \dots, n$.

### B. Bond graph model of a switched reluctance machine

The bond graph model of a SRM is depicted in Fig. 6. It contains two dissipative R-elements (for the electrical, $R \in \mathbb{R}^{n\times n}$, and the mechanical parts, $b \in \mathbb{R}$), two effort sources Se-elements (also electrical and mechanical parts, $V \in \mathbb{R}^n$ and $\tau_L$ respectively), and an I-element which represents the rotor inertia, $J$, of the SRM.

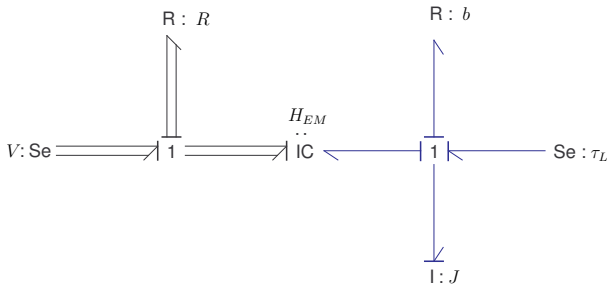


Fig. 6. Bond graph of a switched reluctance machine.

As explained in Section II, the flows and efforts of the IC-field power bonds can be computed from the energy function (7), with $\lambda = p_E \in \mathbb{R}^n$ and $\theta = q_M$,

$$H_{EM} = \frac{1}{2}p_E^T \mathcal{L}^{-1} p_E, \tag{16}$$

For Peer Review

where, in this case, the inductance matrix is defined as (12), *i.e.*, $\mathcal{L} = \mathcal{L}(q_M)$. From (3) and (4),

$$f_E = = \mathcal{L}^{-1} p_E \quad (17)$$

$$e_M = = \frac{1}{2} p_E^T \partial_{q_M}(\mathcal{L}^{-1}) p_E \quad (18)$$

where $\partial_{q_M}(\mathcal{L}^{-1})$ is given by equation (14). Finally the state variables can be obtained from (1) and (2),

$$\dot{p}_E = e_E \quad (19)$$

$$\dot{q}_M = f_M. \quad (20)$$

### C. Simulations

In this section a numerical simulation of the bond graph model for a 6/4 switched reluctance machine, acting as a motor, is implemented using a single pulse mode operation (see Fig. 7). As shown in Fig. 4, this configuration has three stator phases, called $a$, $b$ and $c$. The 20sim software, which allows to implement and simulate bond graph models, is used. The elements are obtained from the standard library, except the IC-element, which is constructed from the standard IC-element by adding the appropriate ports and writing the following code, where `PE.e`=$e_E$, `PM.e`=$e_M$, `PE.f`=$f_E$, `PM.f`=$f_M$,

```
La=lo-l1*cos(Nr*qM);
Lb=lo-l1*cos(Nr*qM+1*pi/3);
Lc=lo-l1*cos(Nr*qM+2*pi/3);
L=[La,0,0;0,Lb,0;0,0,Lc];

diLa=-l1*Nr*sin(Nr*qM)/(lo-l1*cos(Nr*qM))^2;
diLb=
-l1*Nr*sin(Nr*qM+1*pi/3)/(lo-l1*cos(Nr*qM+1*pi/3))^2;
diLc=
-l1*Nr*sin(Nr*qM+2*pi/3)/(lo-l1*cos(Nr*qM+2*pi/3))^2;
diL=[diLa,0,0;0,diLb,0;0,0,diLc];

pE= int (PE.e);

reset = if qM > 2*pi then true else false end;
qM = resint(PM.f,0,reset);
PE.f=inverse(L)*pE;
PM.e=1/2*transpose(PE.f)*diL*PE.f;
```

The machine parameters correspond to the 6/4 SRM used in the next section. The electrical parameters are: the aligned and non-aligned inductances $l_0 = 0.047$H and $l_1 = 0.033$H, respectively, the phase resistance is $r = 2\Omega$, with an estimated friction coefficient of $b = 0.0035$N m rad$^{-1}$s and a rotor inertia (including the inertia of the DC break) $J = 0.0003$kg m$^2$. The bus voltage is fixed at $V = 300$V, and a single pulse three-phase voltage is generated according to the rotor position as explained in Section III. During the simulation test, an external breaking torque $\tau_L = -1.8$N m, has been applied at $t = 0.02$s. To emulate the power converter, an ideal three-phase voltage source is considered. In Fig. 7 the applied phase voltages are depicted.They contain a negative part, used to help to extinguish the phase current in order to avoid over-voltages in the inductors during the commutation.

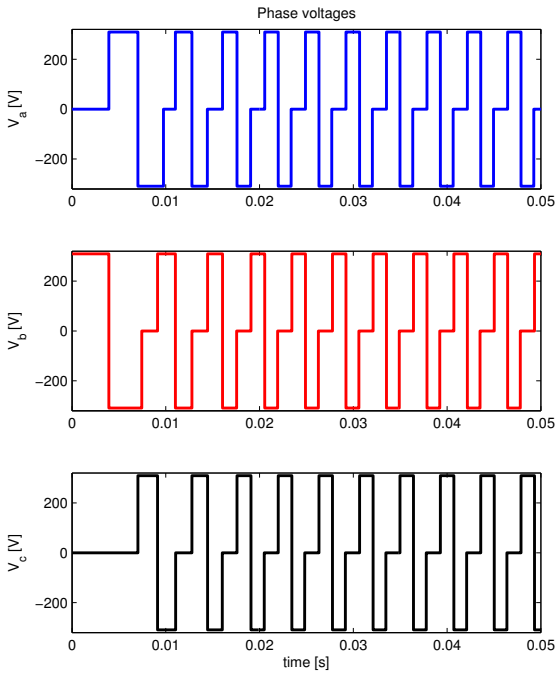


Fig. 7. 6/4 SRM simulation results: phase voltages (single pulse mode operation).

Simulation results are presented in Figures 8 to 10. Figures 8 and 9 show the three-phase currents and a pulse detail of the $a$-phase.

The produced electrical torque, $\tau_e$, and the mechanical speed, $\omega$, are depicted in Fig. 10. The simulated machine is a three-phase machine and, consequently the torque is rippled with a frequency three times the mechanical speed. Also, notice that following the bond graph convention of Fig. 6, the mechanical power of the IC-element must be negative for a motor mode, which implies that the steady-state value of the torque is negative while the mechanical speed is positive (they product, which is power, is then negative).

## V. The Experimentally Based SRM Model

Experimental tests can be carried out in order to obtain the magnetic characteristics of the SRM. From the flux linkage curves, the inductance matrix elements, $\mathcal{L}(\theta, i)$, of (11), can be computed, and consequently the IC-element can be fully defined.

In this section a bond graph model for a 6/4 SRM machine using the flux characteristic curves experimentally obtained from a real machine is presented. The bond graph model is implemented using the 20sim software and its results are compared with real experiments.

### A. Experimental setup

The experimental setup follows the schematic block diagram of the SRM motor drive shown in Fig. 11. The power converter

For Peer Review

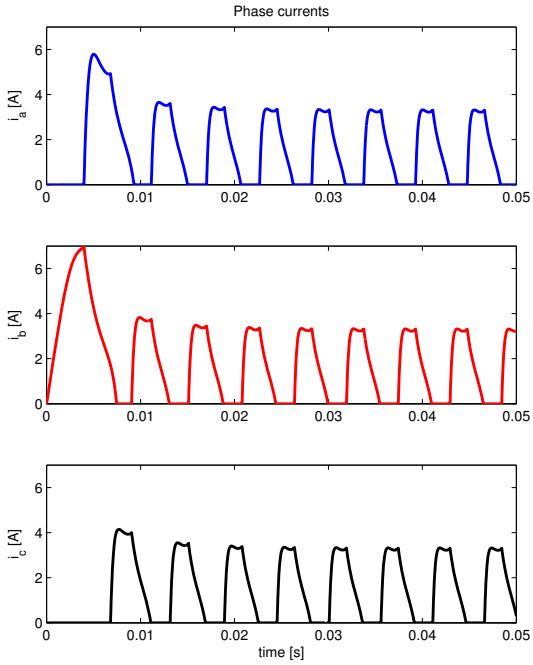


Fig. 8. 6/4 SRM simulation results: Phase currents.

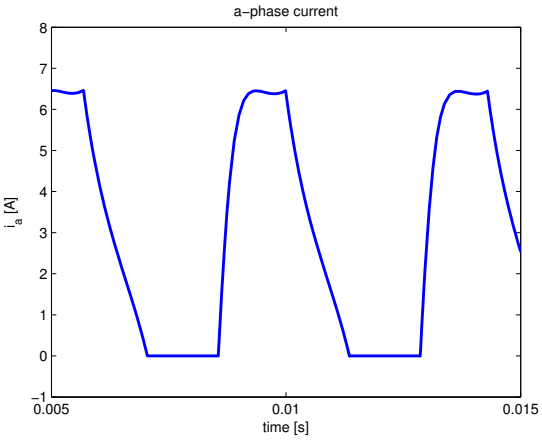


Fig. 9. 6/4 SRM simulation results: detail of the a-phase current.

is a classic converter with two IGBT and two fast diodes per phase connected to the AC supply through a three phase diode bridge rectifier and a capacitor bank. Rotor position signals come from an ensemble formed by a slotted disk and three optointerrupters placed inside the SRM. Current measurements are performed using Hall effect current sensors. Digital control is implemented in the DSPACE ACE kit 1104 CLP, which includes a TMS320F240 DSP.

The machine is a 0.75kW, rated at 2.4Nm at 3000rpm. The sampling time has been selected at 60$\mu$s.

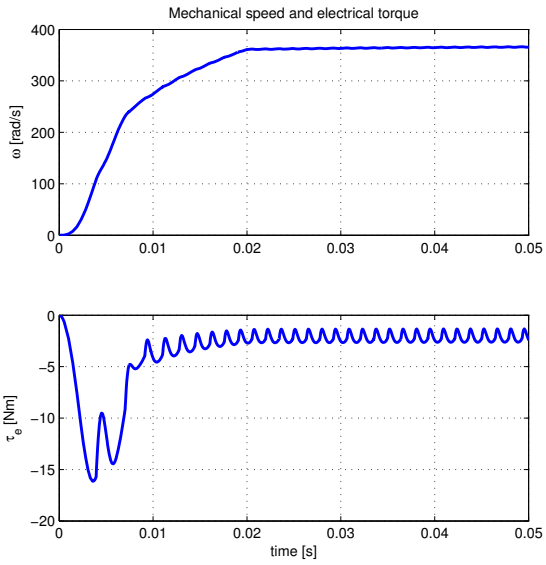


Fig. 10. 6/4 SRM simulation results: Mechanical speed and electrical torque.

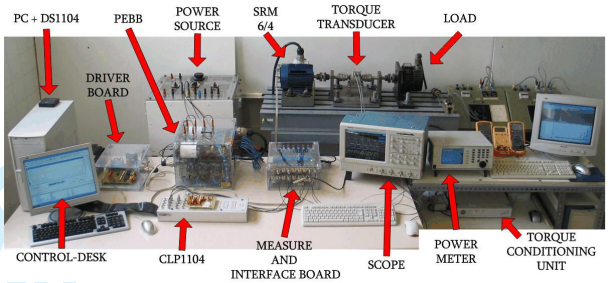


Fig. 11. 6/4 SRM experimental setup.

## B. Experimental curves

Figure 12 show the experimental curves of the flux linkage for a 6/4 SRM, which are obtained for different rotor position, $\theta$, and with a phase current from 1 to 10A.

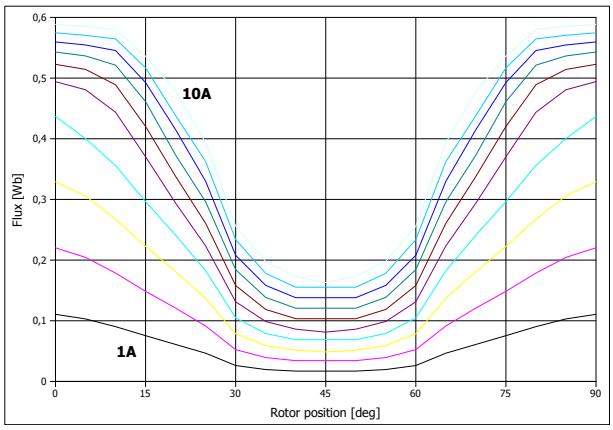


Fig. 12. Flux characteristics for a real 6/4SRM.

The proposed model does not take into account the mutual inductance between phases, and from (6), the matrix induc-

Peer Review

tances can be written as

$$\mathcal{L} = \begin{bmatrix} L_a & 0 & 0 \\ 0 & L_b & 0 \\ 0 & 0 & L_c \end{bmatrix}, \quad (21)$$

where the value of each phase, $L_j$, is obtained from data plotted in Fig. 13, tacking into account the shift angle for each phase. The previous matrix give us the relationship between fluxes and current. From the flux data of Fig. 12 and using (6), is easy to obtain the inductance value, depending on the current and rotor position. Data results for the tested 6/4 SRM are plotted in Fig. 13.

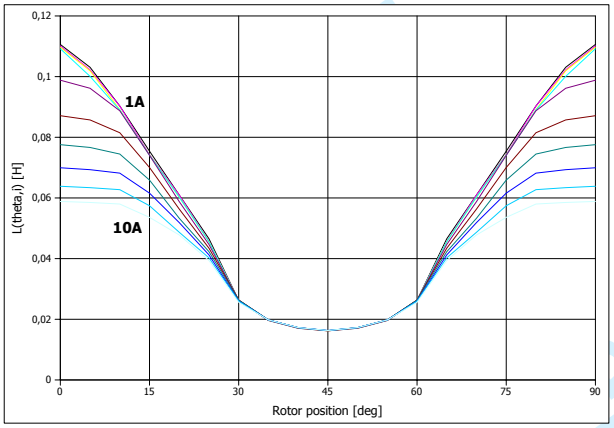


Fig. 13. Inductance value of a SRM, depending on the rotor position and the phase current.

As explained before, the torque is obtained from (10), where the $\partial_\theta(\mathcal{L}^{-1})$ matrix is

$$\partial_\theta(\mathcal{L}^{-1}) = \begin{bmatrix} \partial_\theta(\mathcal{L}_a^{-1}) & 0 & 0 \\ 0 & \partial_\theta(\mathcal{L}_b^{-1}) & 0 \\ 0 & 0 & \partial_\theta(\mathcal{L}_c^{-1}) \end{bmatrix}. \quad (22)$$

The $\partial_\theta(\mathcal{L}_j^{-1})$ values, which depend on the rotor position and the phase current, can be computed by differentiating offline the curves from Fig. 13. In Fig. 14 the curves corresponding to the 6/4 SRM are displayed.

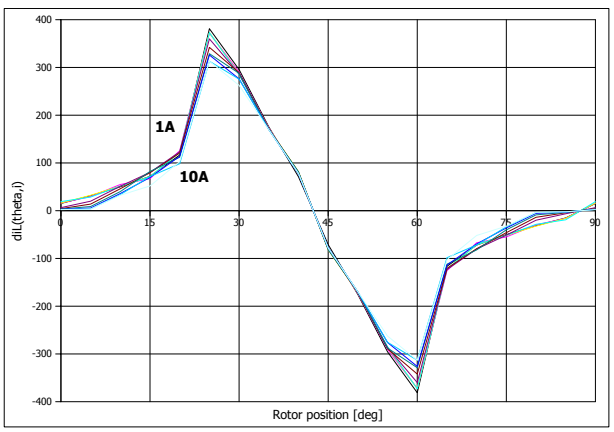


Fig. 14. $\theta$-derivative values of the inverse of inductance values.

### C. The bond graph model

The bond graph model for this case is the same considered for the linear case in Section IV, except for the constitutive equations of the IC-element. Instead of computing analytically the `Lj` and `diLj` values, they are obtained from tables[3] corresponding to Figures 13 and 14. The 20sim implementation of this IC-element is given by

```
Lavalues= [Lid;theta;pE.f[1]];
Lbvalues= [Lid;theta+pi/3;pE.f[2]];
Lcvalues= [Lid;theta+2*pi/3;pE.f[3]];
La=dll ('Table2D.dll', 'TableRead',Lavalues);
Lb=dll ('Table2D.dll', 'TableRead',Lbvalues);
Lc=dll ('Table2D.dll', 'TableRead',Lcvalues);
L=[La,0,0;0,Lb,0;0,0,Lc];

diLavalues= [diLid;theta;pE.f[1]];
diLbvalues= [diLid;theta+pi/3;pE.f[2]];
diLcvalues= [diLid;theta+2*pi/3;pE.f[3]];
diLa=dll ('Table2D.dll', 'TableRead',diLavalues);
diLb=dll ('Table2D.dll', 'TableRead',diLbvalues);
diLc=dll ('Table2D.dll', 'TableRead',diLcvalues);
diL=[diLa,0,0;0,diLb,0;0,0,diLc];

pE= int (PE.e);

reset = if qM > 2*pi then true else false end;
qM = resint(PM.f,0,reset);
PE.f=inverse(L)*pE;
PM.e=1/2*transpose(PE.f)*diL*PE.f;
```

### D. Simulations and experimental results comparison

In order to validate the proposed model a real experiment is reproduced in a simulation test. The real SRM is controlled with a single pulse operation mode, using a bus voltage of $V = 309$V, and with an external torque of $\tau_L = 1.8$N m. In steady state, the SRM reaches a constant speed of $\omega = 3514$rpm.

This experiment is then compared with simulations of the two bond graph models described above. Using the parameters given in the previous Section and tables obtained from the SRM, the bond graph models are ran within the 20sim simulation environment.

Fig. 15 shows the a-phase current waveform in steady state. Note that both bond graph models produce a similar real current shape. The experimentally based model offers the main advantage of including saturation effects, as well as a more realistic scenario. The main problem found using the *look at table* model are the discontinuities of the $\partial_\theta(\mathcal{L}_j^{-1})$ values. This problem can be avoid using an analytic model, which ensures an smooth behaviour of the $\mathcal{L}$ values, or minimized with a large data table increasing the flux measures.

[3]In this case, a linear interpolation is used.

For Review

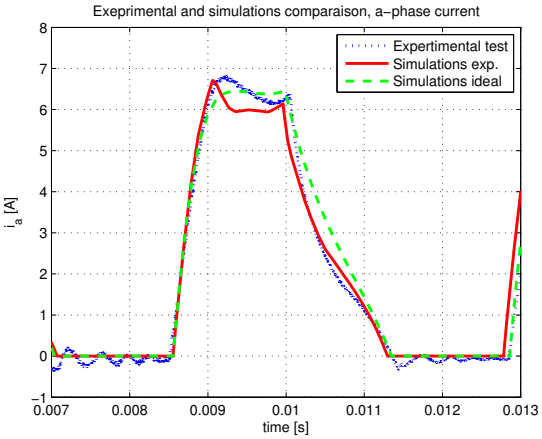


Fig. 15. 6/4 SRM experimental and simulation comparison: a-phase electric current for the real SRM machine, the classic-based SRM bond graph model and the experimentally-based SRM bond graph model.

## VI. Conclusions

A bond graph model of a switched reluctance machine is presented. Using an IC-element, and defining an energy function, the SRM is simulated and the simulation results are compared with a real system.

Thanks to the energy-based description of the bond graph, saturation effects are easily included by replacing the analytic functions of the IC-element by data experimentally obtained. Numerical simulations are compared with experimental results obtained from a real SRM, and the model is validated.

Furthermore, the bond graph approach describes physically the system and does not assume a given mode of operation, as the same model can be reused for motor or generator applications.

## References


[1] T. Miller, *Electronic control of Switched Reluctance Machines*, 1st ed. Prentince-Hall, 2001.

[2] K. Rahman, B. Fahimi, G. Suresh, A. Rajarathnam, and M. Ehsani, "Advantages of switched reluctance motor applications to ev and hev: design and control issues," *IEEE Trans. on Industry Applications*, vol. 36, no. 1, pp. 111–121, 2000.

[3] R. Cárdenas, R. Peña, M. Pérez, J. Clare, G. Asher, and P. Wheeler, "Power smoothing using a flywheel driven by a switched reluctance machine," *IEEE Trans. on Industrial Electronics*, vol. 53, no. 4, pp. 1086–1093, 2006.

[4] I. Husain, "Minimization of torque ripple in srm drives," *IEEE Trans. on Industrial Electronics*, vol. 49, no. 1, pp. 28–39, 2002.

[5] I. Husain and S. Hossain, "Modeling, simulation and control of switched reluctance motor drives," *IEEE Trans. on Industrial Electronics*, vol. 52, no. 6, pp. 1625–1634, 2005.

[6] L. Belfore and A. Arkadan, "Modeling faulted switched reluctance motors using evolutionary neural networks," *IEEE Trans. on Industral Electronics*, vol. 44, no. 2, pp. 226–233, 1997.

[7] A. Jain and N. Mohan, "Dynamic modeling, experimental characterization, and verification for srm operation with simultaneous two-phase excitation," *IEEE Trans. on Industrial Electronics*, vol. 53, no. 4, pp. 1238–1249, 2006.

[8] C. Edrington, B. Fahimi, and M. Krishnamurthy, "An autocalibrating inductance model for switched reluctance motor drives," *IEEE Trans. on Industrial Electronics*, vol. 54, no. 4, pp. 2165–2173, 2007.

[9] P. Gawthrop and G. Bevan, "Bond-graph modeling," *IEEE Control Systems Magazine*, vol. 27, no. 2, pp. 24–45, 2007.

[10] D. Karnopp, D. Margolis, and R. Rosenberg, *System dynamics modeling and simulation of mechatronic systems*, 3rd ed. J. Wiley, New York, 2000.

[11] A. Vaz and S. Hirai, "A bond graph approach to the analysis of prosthesis for a partially impaired hand," *ASME Journal of Dynamic Systems, Measurement, and Control*, vol. 129, pp. 105–113, 2007.

[12] R. Redfield, "Bond graphs of open systems: a water rocket example," *IMechE J. Systems and Control Engineering, Part I*, vol. 220, pp. 607–615, 2006.

[13] M. Delgado and H. Sira-Ramirez, "Modeling and simulation of a switch regulated DC-to-DC power converters of the boost type," in *IEEE Proc. Conf. on Devices, Circuits and Systems*, 1995, pp. 84–88.

[14] D. Margolis and T. Shim, "A bond graph model incorporating sensors, actuators, and vehicle dynamics for developing controllers for vehicle safety," *Journal of the Franklin Institute*, vol. 338, pp. 21–34, 2001.

[15] M. Filippa, C. Mi, J. Shen, and R. Stevenson, "Modeling of a hybrid electric vehicle powertrain test cell using bond graphs," *IEEE Trans. on Vehicular Technology*, vol. 54, no. 3, pp. 837–845, 2005.

[16] G. Gandanegara, X. Roboam, B. Sareni, and G. Dauphin-Tanguy, "Bond-graph-based model simplification for system analysis: application to a railway traction device," *IMechE J. Systems and Control Engineering, Part I*, vol. 220, pp. 553–571, 2006.

[17] C. Batlle and A. Dòria-Cerezo, "Bond graph models of electromechanical systems. the ac generator case," in *Proc. IEEE Int. Symp. on Industrial Electronics*, 2008.

[18] J. Kim and M. Bryant, "Bond graph model of a squirrel cage induction motor with direct physical correspondence," *ASME Journal of Dynamic Systems, Measurement, and Control*, vol. 122, pp. 461–469, September 2000.

[19] B. Umesh-Rai and L. Umanand, "Bond graph toolbox for handling complex variable," *IET Control Theory and Applications*, vol. 3, no. 5, pp. 551–560, 2009.

[20] J. Campos, M. Crawford, and R. Longoria, "Rotordynamic modeling using bond graphs: modeling the jeffcott rotor," *IEEE Trans. on Magnetics*, vol. 41, no. 1, pp. 274–280, 2005.

[21] M. Hecquet and P. Brochet, "Modeling of a claw-pole alternator using permeance network coupled with electric circuits," *IEEE Trans. on Magnetics*, vol. 31, no. 3, pp. 2131–2134, 1995.

[22] C. Delforge and B. Lemaire-Semail, "Induction machine modeling using finite element and permeance network methods," *IEEE Trans. on Magnetics*, vol. 31, no. 3, pp. 334–339, 1995.

[23] P. Krause, O. Wasynczuk, and S. Sudhoff, *Analysis of Electric Machinery and Drive Systems*. John Wiley & Sons Inc., 2002.


For Peer Review